Chapter 3

Mathematical analysis of the ordinary reflectance scanning microscope

In this chapter the mathematical framework for modelling the reflectance scanning microscope is described in detail. Many authors have presented mathematical analysis describing imaging in optical systems, the forerunner of which was Hopkins who described the imaging process in partially coherent optical systems [44,45]. Hopkins' work was further adapted and applied to the case of imaging in ordinary (simple reflectance and transmission) scanning laser microscopes by Sheppard and Wilson and their co-workers in the 1970s and 1980s [4,5,6,46].

3.1 The ordinary reflectance scanning microscope

The analysis begins with an introduction of the simple scanning microscope illustrated in Fig. 3.1, a configuration that has been extensively studied by others [4,5,6,44,45,46]. However, it is instructive to begin with a review of such a simple configuration since this introduces many of the basic concepts used to treat the more complicated imaging systems of interest in this thesis.

Optical configuration

Illustrated in Fig. 3.1 is the optical layout of the simple ordinary reflectance scanning microscope. The standard optical head of the reflectance scanning microscope comprises an objective lens (Obj), collector lens (Col), and large area photo-detector (Det). Although Fig. 3.1 illustrates the microscope operating in transmission, the same analysis can be applied to a system operating in reflection, in which case the objective

and collector lenses are one and the same, and a beamsplitter is placed prior to the objective lens to separate the incident and reflected beams.

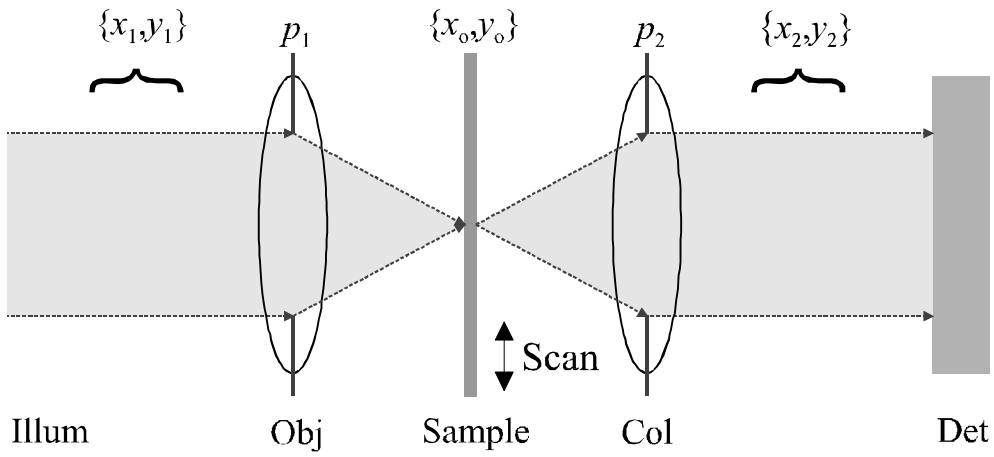

Figure 3.1 : *The optical layout of the ordinary reflectance scanning microscope.*

Scanning is performed in scanning microscopes using two main techniques: beam scanning and sample scanning. In beam scanning systems the focused spot is scanned across a stationary sample, whereas in sample scanning systems the sample is scanned under a stationary focused spot. In the current analysis it is assumed that the sample scanning technique is used to image the sample, thus eliminating the optical complexities evident in beam scanning systems [8].

The objective lens, with associated aperture pupil function $p_1(x_1, y_1)$, focuses a collimated plane wave onto the surface of the sample. The focused field interacts with the sample and then propagates to the collector lens by the diffraction process. The form of the resultant field after interaction with the sample depends upon the reflection / transmission properties of the sample about the scan position. At the plane of the collector lens the field is modified by the aperture pupil function of the collector lens, $p_2(x_2, y_2)$, is collimated and propagates, without further modification, to the large area photo-detector where the signal is generated by the integral, over the area of the photo-detector, of the square magnitude of the incident amplitude field distribution.

Image calculation

The aim of the modelling process is to calculate the electric field distribution, $y'(x_2, y_2)$, in the plane of the photo-detector for a known incident field distribution, $y(x_1, y_1)$, on the objective aperture.

The field distribution, $y(x_o, y_o)$, in the plane of the sample (the focal point of the objective lens) is given by the two-dimensional Fourier transform of the field, $y'(x_1, y_1)$, immediately after the plane of the objective aperture, which following the analysis described in sec. 2.4 gives

$$y(x_o, y_o) = \frac{1}{l f} \Psi\left(\frac{x_o}{l f}, \frac{y_o}{l f}\right) = h_1(x_o, y_o) \tag{3.1}$$

where $h_1(x_o, y_o)$ is the amplitude point spread function of the objective lens, and all other symbols have their usual meaning. An important note is that in the current analysis it is assumed that the objective lens is in perfect focus and is free of aberrations; detractions from such ideal conditions that result in signal degradation which will be treated in detail in later chapters. The field immediately after interaction with the sample, whether operating in reflection or transmission, is given by

$$\begin{aligned} y'(x_o, y_o) &= y(x_o, y_o) r(x_o - x_s, y_o - y_s) \\ &= h_1(x_o, y_o) r(x_o - x_s, y_o - y_s) \end{aligned} \tag{3.2}$$

where $r(x_o, y_o)$ represents the complex amplitude reflectance, or transmittance, of the sample about the scan position, (x_s, y_s). After reflection from the surface of the sample the field propagates towards the collector lens by the diffraction process. The field, $y(x_2, y_2)$, in the plane of the collector lens is given by the two-dimensional Fourier transform of the field, $y'(x_o, y_o)$, immediately after interaction with the sample. Hence, the field at the collector lens [4,7,20] is given by

$$\begin{aligned} y(x_2, y_2) &= \frac{1}{l f} \iint_{-\infty}^{\infty} y'(x_o, y_o) \exp\left\{\frac{jk}{f}(x_2 x_o + y_2 y_o)\right\} dx_o dy_o \\ &= \frac{1}{l f} \iint_{-\infty}^{\infty} h_1(x_o, y_o) r(x_o - x_s, y_o - y_s) \exp\left\{\frac{jk}{f}(x_2 x_o + y_2 y_o)\right\} dx_o dy_o \end{aligned} \tag{3.3}$$

in which phase factors have been ignored, f is the focal length of the collector lens, which is assumed to be equal to the focal length of the objective lens, and all other symbols have their usual meaning. The effect of the collector lens is to collimate the diverging reflected wave by introducing a phase factor into the optical field. However, to simplify the current analysis the phase introduced by the lens has been ignored. The field, $y'(x_2, y_2)$, immediately after the collector lens is given by the multiplication of the incident field distribution, $y(x_2, y_2)$, and the collector aperture pupil function, $p_2(x_2, y_2)$, i.e.

$$y'(x_2, y_2) = y(x_2, y_2) p_2(x_2, y_2) \tag{3.4}$$

this field then propagates, without further modification, towards the large area photo-detector. The signal from the photo-detector, as a function of scan position, is given by the integral, over the area of the photo-detector, of the square magnitude of the incident field distribution, i.e.

$$I(x_s, y_s) = \iint_{-\infty}^{\infty} |y'(x_2, y_2)|^2 R(x_d, y_d) dx_d dy_d \Big|_{x_d = x_2, y_d = y_2} \tag{3.5}$$

where $R(x_d, y_d)$ represents the responsivity of the photo-detector. Assuming the responsivity of the photo-detector is uniform (and set to unity) then the signal from the photo-detector, as a function of scan position, is given by

$$I(x_s, y_s) = \iint_{-\infty}^{\infty} |y(x_2, y_2) p_2(x_2, y_2)|^2 dx_2 dy_2 \tag{3.6}$$

which by expanding gives

$$I(x_s, y_s) = \iint_{-\infty}^{\infty} y(x_2, y_2) y^*(x_2, y_2) |p_2(x_2, y_2)|^2 dx_2 dy_2 \ . \tag{3.7}$$

Substituting for $y(x_2, y_2)$ from eq. (3.3) gives

$$\begin{aligned} I(x_s, y_s) = & \iint_{-\infty}^{\infty} |p_2(x_2, y_2)|^2 \\ & \cdot \frac{1}{lf} \iint_{-\infty}^{\infty} h_1(x_o, y_o) r(x_o - x_s, y_o - y_s) \exp\left\{\frac{jk}{f}(x_2 x_o + y_2 y_o)\right\} dx_o dy_o \\ & \cdot \frac{1}{lf} \iint_{-\infty}^{\infty} h_1^*(x_o', y_o') r^*(x_o' - x_s, y_o' - y_s) \exp\left\{\frac{-jk}{f}(x_2 x_o' + y_2 y_o')\right\} dx_o' dy_o' \\ & \cdot dx_2 dy_2 \end{aligned} \tag{3.8}$$

where x_o' and y_o' are dummy variables introduced to satisfy the multiplication of y and y^*. Rearranging eq. (3.8) gives

$$I(x_s, y_s) = \iint_{-\infty}^{\infty} h_1(x_o, y_o) r(x_o - x_s, y_o - y_s) h_1^*(x_o', y_o') r^*(x_o' - x_s, y_o' - y_s) \cdot \iint_{-\infty}^{\infty} |p_2(x_2, y_2)|^2 \exp\left\{\frac{jk}{f}\left(x_2(x_o - x_o') + y_2(y_o - y_o')\right)\right\} dx_2 dy_2 \cdot dx_o dy_o dx_o' dy_o' \quad (3.9)$$

where constant scaling factors have been ignored. Equation (3.9) can be further simplified to give

$$I(x_s, y_s) = \iint_{-\infty}^{\infty} h_1(x_o, y_o) r(x_o - x_s, y_o - y_s) \cdot h_1^*(x_o', y_o') r^*(x_o' - x_s, y_o' - y_s) \cdot g_2(x_o - x_o', y_o - y_o')\, dx_o\, dy_o\, dx_o' dy_o' \quad (3.10)$$

where $g_2(x_o, y_o)$ is the point spread function associated with the square magnitude of the collector aperture pupil function [4,7,20], given by

$$g_2(x_o, y_o) = \iint_{-\infty}^{\infty} |p_2(x_2, y_2)|^2 \exp\left\{\frac{jk}{f}\left(x_o x_2 + y_o y_2\right)\right\} dx_2 dy_2 \quad (3.11)$$

where *f* is the focal length of the collector lens and all other symbols have their usual meaning.

Equation (3.10) is a convolution type process involving the objective amplitude point spread function, h_1, the object reflectance, *r*, and the point spread function associated with the square modulus of the collector pupil function, g_2.

It is useful at this point to consider two extreme cases of collector aperture size that govern the operation of the reflectance scanning microscope. These two cases are referred to as ***coherent*** and ***incoherent*** imaging [4,7,20].

3.1.1 The coherent optical channel

Consider the situation where the collector aperture is very small, such that it may be described by a delta function [4,7,20]. In this case, the amplitude point spread function, g_2, becomes

$$g_2(x_o, y_o) = 1 \tag{3.12}$$

which by substituting into eq. (3.10) and rearranging gives

$$I(x_s, y_s) = \left[\iint_{-\infty}^{\infty} h_1(x_o, y_o) r(x_o - x_s, y_o - y_s)\, dx_o dy_o \right] \cdot \iint_{-\infty}^{\infty} h_1^*(x_o', y_o')\, r^*(x_o' - x_s, y_o' - y_s)\, dx_o' dy_o' \tag{3.13}$$

Equation (3.13) can be expressed in the simplified form

$$I(x_s, y_s) = \left| h_1(x_s, y_s) \otimes r(-x_s, -y_s) \right|^2 \tag{3.14}$$

where $\otimes$ represents convolution. The resulting signal from the reflectance scanning microscope is now linear in field amplitude and is generally termed ***coherent*** imaging. The negative signs in eq. (3.14) indicate that strictly eq. (3.13) is in the form of a correlation integral. Equation (3.14) illustrates that the response of the coherent scanning microscope is generated by calculating the square magnitude of the convolution of the objective amplitude point spread function and the reflectance characteristics of the sample.

Step response

Figure 3.2 illustrates the normalised step response of the coherent scanning microscope for a clear, aberration free, circular objective aperture under uniform illumination. The response has been generated using the transfer function model described in chapter 6.

An important characteristic of coherent imaging is evident in Fig. 3.2. The response of the coherent imaging system exhibits undesirable ringing and a lag in the response to a straight edge. It has been the work of many researchers to apply apodization

techniques to remove the undesired ringing from the coherent response whilst maintaining the fastest rise time [4,7].

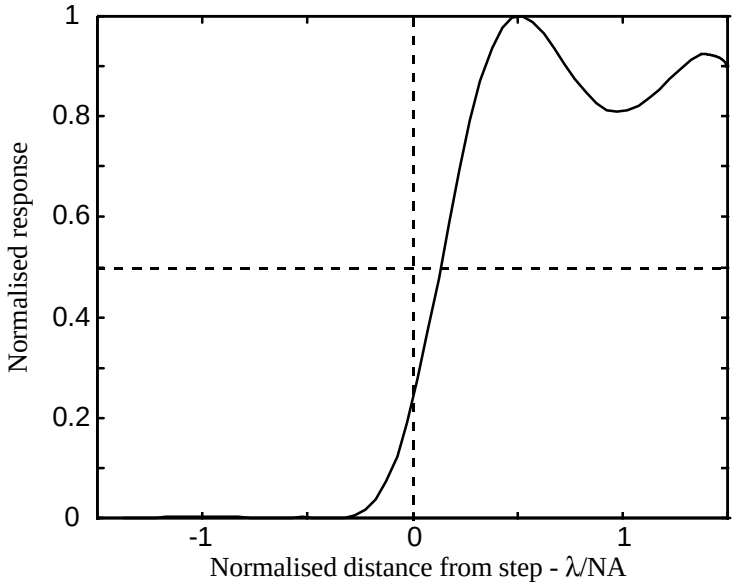

Figure 3.2 : *The normalised step response of the coherent scanning microscope, for a clear, aberration free, circular objective under uniform illumination.*

3.1.2 The incoherent optical channel

Consider the situation where the collector aperture is infinitely large [4,7,20], such that the aperture pupil function, $p_2(x_2, y_2)$, is constant, and the associated amplitude point spread function is effectively a delta function,

$$g_2(x_o, y_o) = d\,(x_o, y_o)\ . \tag{3.15}$$

Substituting into eq. (3.10) gives

$$\begin{aligned} I(x_s, y_s) = \iint_{-\infty}^{\infty} & h_1(x_o, y_o) r\,(x_o - x_s, y_o - y_s) \\ & \cdot\ h_1{}^*(x_o, y_o)\ r^*(x_o - x_s, y_o - y_s)\ dx_o dy_o \end{aligned} \tag{3.16}$$

which can be expressed in the simplified form

$$I(x_s, y_s) = \left|h_1(x_s, y_s)\right|^2 \otimes \left|r(-x_s, -y_s)\right|^2 \tag{3.17}$$

where $\otimes$ represents convolution. It can be seen from eq. (3.17) that the signal from the reflectance scanning microscope is now linear in the square modulus of the electric field amplitude, the irradiance, and so is generally termed ***incoherent*** imaging. Equation (3.17) illustrates that the response of the incoherent scanning microscope is

generated by the convolution (strictly correlation) of the square magnitude of the objective point spread function and the square magnitude of the reflectance properties of the sample.

Step response

Figure 3.3 illustrates the normalised step response of the incoherent scanning microscope for a clear, aberration free, circular objective aperture under uniform illumination. The response has been generated using the transfer function model described in chapter 6. It can be seen that the response is very different to that of the coherent system. The response of the incoherent imaging system exhibits none of the undesirable ringing characteristics of the coherent imaging system, and, unlike the coherent system, the response to a straight edge is symmetrical about the centre of the edge.

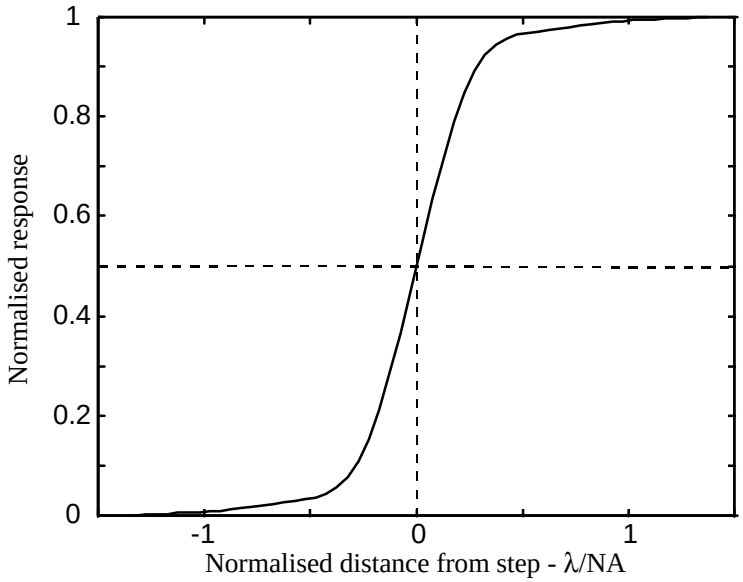

Figure 3.3 : *The normalised step response of the incoherent scanning microscope, for a clear, aberration free, circular objective under uniform illumination.*

The simple incoherent imaging model, often referred to as the ***convolutional model***, is often used by researchers to calculate the theoretical readout signal in optical disc systems, due to the fact that experimental observations agree very closely with predictions of the incoherent model [18,48,49,50,51].

The incoherent transfer function

It is common to characterise the performance of electrical systems in terms of their impulse response, step response or frequency response. In electrical systems the variable of interest is temporal frequency, and it is with this that transfer function representations of electrical circuits can be developed. In order to evaluate the frequency response of the optical imaging system, a transfer function representation has to be developed. In optical systems the variable of interest is spatial frequency, and hence this can be used to characterise their transfer function behaviour.

The optical impulse can be represented by a point object, which can be visualised as a delta function, i.e.

$$r(x,y) = d(x,y) \tag{3.18}$$

which by substituting into eq. (3.17) gives

$$I(x_s, y_s) = \left| h_1(x_s, y_s) \right|^2 \tag{3.19}$$

which is the impulse response of the incoherent imaging system. If the objective is a clear, aberration free, circular aperture under uniform illumination, then the impulse response of the incoherent system is given by the well known *Airy disc* pattern of eq. (2.23) which is illustrated in Fig. (2.2) [4,6,7,20,46].

The ***optical transfer function***, **OTF**, is the spatial frequency representation of the frequency response of the optical imaging system [40,44]. The incoherent OTF is given by the two-dimensional Fourier transform of the incoherent impulse response. Therefore, the incoherent OTF is given by

$$O(n_x, n_y) = \iint_{-\infty}^{\infty} \left| h_1(x_o, y_o) \right|^2 \exp\left\{ 2p\, j\left(x_o n_x + y_o n_y \right) \right\} dx_o\, dy_o \tag{3.20}$$

where n_x and n_y are spatial frequency components in the x and y directions respectively. However, the amplitude point spread function is simply the two-dimensional Fourier transform of the aperture pupil function of the objective lens. Therefore, substituting for $h_1(x_1, y_1)$ from eq. (3.1) into eq. (3.20) gives

$$O(n_x, n_y) = \iint_{-\infty}^{\infty} \left(\frac{1}{l f}\right)^2 P_1\left(\frac{x_o}{l f}, \frac{y_o}{l f}\right) P_1 * \left(\frac{x_o}{l f}, \frac{y_o}{l f}\right) \cdot \exp\left\{2p j\left(x_o n_x + y_o n_y\right)\right\} dx_o dy_o \tag{3.21}$$

where p_1 and P_1 are Fourier transform pairs and * represents complex conjugation. Using Fourier transform theorems eq. (3.21) can be represented as a function of the objective aperture pupil function and its complex conjugate [4,42,43], i.e.

$$O(n_x, n_y) = \iint_{-\infty}^{\infty} p_1\left(x + n_x l f, y + n_y l f\right) p_1 * (x, y) \; dxdy \tag{3.22}$$

or in short form,

$$O(n_x, n_y) = p_1\left(n_x l f, n_y l f\right) \otimes p_1 * \left(-n_x l f, -n_y l f\right) \tag{3.23}$$

where $\otimes$ represents two-dimensional convolution and all other symbols have the usual meaning. It can seen that the incoherent optical transfer function is given by the two-dimensional convolution of the aperture pupil function and its reversed complex conjugate. For a clear, aberration free, circular objective aperture under uniform illumination, and a specific pair of spatial frequencies n_x and n_y, the incoherent OTF is equivalent to the area of overlap of two circles, one centred about the origin and the other displaced by $n_x l f$ in the x - direction, and $n_y l f$ in the y - direction, as illustrated in Fig. 3.4.

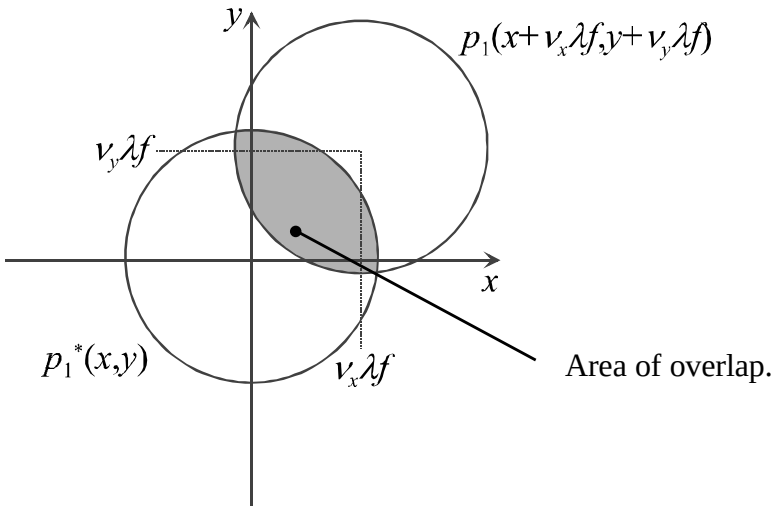

Figure 3.4 : *Generation of the incoherent optical transfer function by the calculation of the area of overlap of the displaced circular objective pupil function and its complex conjugate centred about the origin.*

In this example where the objective is devoid of any aberrations, the OTF is purely real. However, in aberrated systems the OTF is in fact complex, having both magnitude and phase. The magnitude of the OTF is referred to as the ***modulation transfer function***, ***MTF***, and the phase of the OTF is referred to as the ***phase transfer function***, ***PTF*** [32,43,52].

Figure 3.5 illustrates the calculated incoherent OTF for a clear, aberration free, circular objective aperture under uniform illumination, where the frequency axes are given in normalised spatial frequency components

$$n_N = \frac{n\,l}{NA} \tag{3.24}$$

where l is the wavelength of illumination, and NA is the numerical aperture of the objective lens [4,20].

The cut-off in the OTF (i.e. $O(n_x, n_y) = 0$) occurs at the characteristic spatial frequency

$$n_c = \sqrt{n_x^2 + n_y^2} = 2\frac{NA}{l} \tag{3.25}$$

which corresponds to a displacement of p_1 of one diameter in any direction, at which point the circles in Fig. 3.4 no longer overlap. The incoherent OTF illustrated in Fig. 3.5 has the well known form given by

$$O\left(n_x, n_y\right) = \frac{2}{p}\left(\cos^{-1}\left(\frac{n}{2}\right) - \frac{n}{2}\sqrt{1-\left(\frac{n}{2}\right)^2}\right) \qquad n \le 2; \qquad n = \frac{2lf}{d}\sqrt{\left(n_x^2 + n_y^2\right)} \tag{3.26}$$

where d is the diameter of the circular objective aperture, and all other symbols have their usual meaning.

Figure 3.6 illustrates the effects that the form of the incident illumination can have on the spatial frequency characteristics of the incoherent imaging system. Plots are illustrated along the n_x axis of the incoherent OTF, for a clear, aberration free, circular objective aperture, under both uniform illumination and Gaussian illumination ($w_{e^{-2}} = a/2$, a - aperture radius).

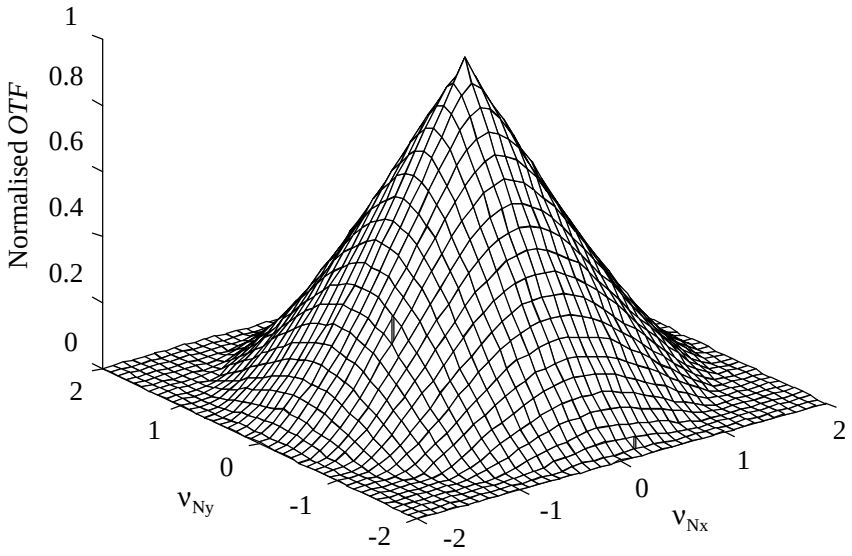

Figure 3.5 : *The incoherent optical transfer function, for a clear, aberration free, circular objective aperture under uniform illumination.*

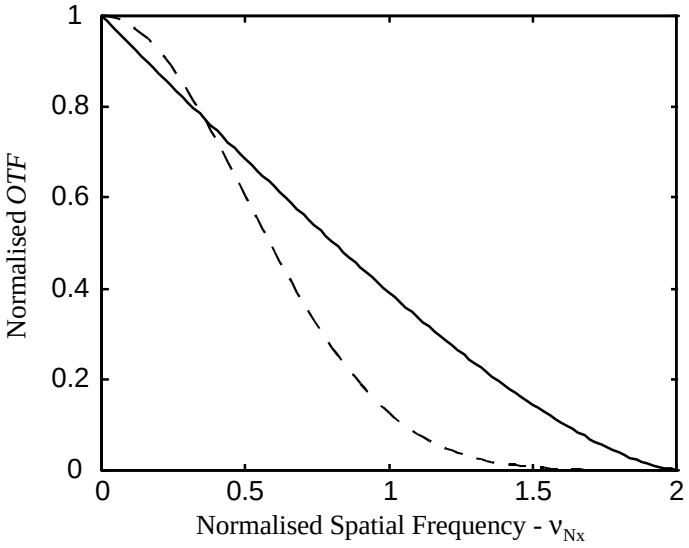

Figure 3.6 : *Plot along the n_x axis of the incoherent OTF for uniform illumination (solid line) and Gaussian illumination ($w_{e^{-2}} = a/2$) (dashed line), for a clear, aberration free, circular objective aperture.*

It is clear that the response and the shape of the incoherent OTF depends significantly on the form of the incident illumination and the shape of the objective aperture. In the case of uniform illumination and a circular objective aperture (solid line) the transfer function rolls off at an approximately linear rate (actually as in eq. (3.26)) with

increase in spatial frequency. However, in the case of Gaussian illumination ($w_{e^{-2}} = a/2$) and a circular aperture the shape of the OTF has changed dramatically, with a boost of the low spatial frequency response and the attenuation of the high spatial frequency response.

3.1.3 Coherence ratio

The coherence ratio [32], g, is defined as the ratio of the numerical aperture of the collector lens to the numerical aperture of the objective lens, i.e.

$$g = \frac{NA_C}{NA_O} \tag{3.27}$$

where the subscripts O and C refer to the objective and collector lenses respectively. For the coherent optical system where the collector aperture pupil function is infinitesimally small, the coherence ratio is $g = 0$, and for the incoherent imaging system where the collector aperture pupil function is infinitely large, the coherence ratio is $g = \infty$.

It can be shown that the spatial frequency cut-off of the OTF is a function of the coherence ratio of the imaging system, and can be expressed as

$$\begin{aligned} n_c &= (1+g)\frac{NA}{l} && 0 \le g \le 1 \\ n_c &= \frac{2NA}{l} && g \ge 1 \end{aligned} \quad . \tag{3.28}$$

Figure 3.7 illustrates the effect that the size of the collector aperture has on the spatial frequency response and the resolving power of the ordinary reflectance system. It can be seen that the coherent imaging system cuts off at half the spatial frequency of the incoherent system and that it has a flat frequency response within the low spatial frequency region. An interesting result is that for a coherence factor of $g \ge 1$ the spatial frequency cut-off of the imaging system remains constant.

A coherence factor of $g = 1$ is the case where the numerical apertures of the objective and collector lenses are the same. The case where $0 < g < \infty$ corresponds to the case

of the more general partially coherent imaging system which will be treated in detail in sec. 3.2.

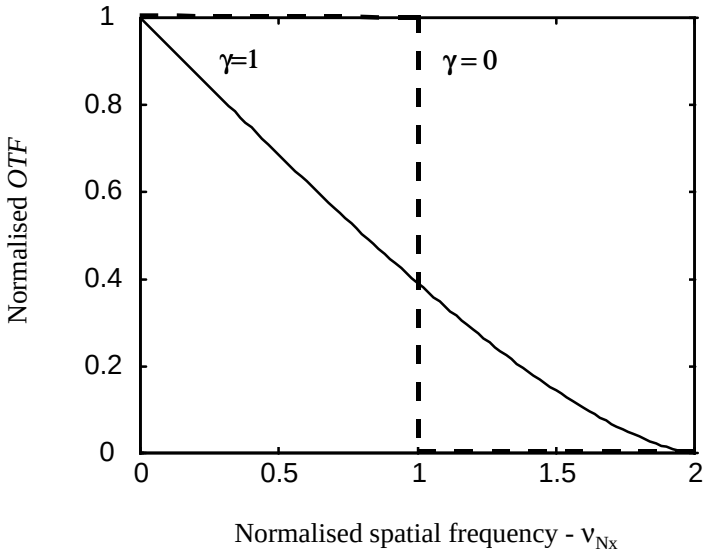

Figure 3.7 : *Plot along the n_x axis of the OTF for a coherence factor of g=0 (bold dashed line) (coherent system) and a coherence factor of g=1 (solid line).*

3.2 The Type 1 reflectance scanning microscope

It has been shown that when the reflectance scanning microscope employs an infinitesimally small collector aperture or an infinitely large collector aperture, then the characteristics of the imaging system are very different. However, it is of more interest to consider the case when the collector aperture is neither infinite in extent nor infinitesimally small in extent, in which case the imaging is neither incoherent or coherent, but partially coherent.

The optical system illustrated in Fig. 3.1 is often referred to as the Type 1 ordinary, reflectance scanning microscope, and it has been discussed in Chap. 1 that it has imaging characteristics similar to that of the conventional microscope. Following the previous analysis, it can be seen that the expression representing the signal from the Type 1 reflectance scanning microscope is given by eq. (3.10), where the collector aperture pupil function, $p_2(x_2, y_2)$ is of finite areal size. It is also useful to develop a transfer function description for this more general, partially coherent, case.

Transfer function representation

To derive a transfer function representation for the signal generated in the Type 1 reflectance scanning microscope, eq. (3.10), then the reflectance properties of the sample must be expressed in terms of its spatial frequency spectrum, $\Gamma(n_x, n_y)$, i.e.

$$r(x, y) = \iint_{-\infty}^{\infty} \Gamma(n_x, n_y) \exp\left(-2p\, j\left[n_x x + n_y y\right]\right) dn_x dn_y \tag{3.29}$$

and its complex conjugate

$$r^*(x, y) = \iint_{-\infty}^{\infty} \Gamma^*(n_x, n_y) \exp\left(2p\, j\left[n_x x + n_y y\right]\right) dn_x dn_y \tag{3.30}$$

where n_x and n_y are spatial frequencies in the x and y directions respectively. Substituting for $r(x, y)$ and $r^*(x, y)$ into eq. (3.10) and rearranging gives

$$\begin{aligned} I(x_s, y_s) = \iint \iint_{-\infty}^{\infty} \Bigg[\iint \iint_{-\infty}^{\infty} & h_1(x_o, y_o)\, h_1^*(x_o', y_o')\, g_2(x_o - x_o', y_o - y_o') \\ & \cdot \exp\left\{-2p\, j\left(n_x x_o - n_x' x_o' + n_y y_o - n_y' y_o'\right)\right\} dx_o\, dy_o\, dx_o'\, dy_o' \Bigg] \\ & \cdot \Gamma(n_x, n_y)\, \Gamma^*(n_x', n_y') \exp\left\{+2p\, j\left(\left(n_x - n_x'\right)x_s + \left(n_y - n_y'\right)y_s\right)\right\} \\ & \cdot dn_x\, dn_y\, dn_x'\, dn_y' \end{aligned} \tag{3.31}$$

where the symbols have their usual meaning. Replacing the term in the square brackets of eq.(3.31) with the function $C(n_x, n_y; n_x', n_y')$, the signal from the Type 1 reflectance system can be expressed in the form

$$\begin{aligned} I(x_s, y_s) = \iint \iint_{-\infty}^{\infty} & C(n_x, n_y; n_x', n_y')\, M(n_x, n_y; n_x', n_y') \\ & \cdot \exp\left\{2p\, j\left[\left(n_x - n_x'\right)x_s + \left(n_y - n_y'\right)y_s\right]\right\} dn_x\, dn_y\, dn_x'\, dn_y' \end{aligned} \tag{3.32}$$

where the function $C(n_x, n_y; n_x', n_y')$ is termed the ***partially coherent transfer function***, **PCTF**, which is a function of the properties of the optical system itself. It describes the intensity of the components in the image with spatial frequencies equal to $(n_x - n_x')$ in the x direction, and $(n_y - n_y')$ in the y direction. The term

$M(n_x, n_y; n_x', n_y')$ is called the medium function and describes the spatial frequency properties of the sample, in this case given by

$$M(n_x, n_y; n_x', n_y') = \Gamma(n_x, n_y)\Gamma^*(n_x', n_y') \quad . \tag{3.33}$$

The Type 1 PCTF

Comparing eq. (3.32) and eq. (3.31), it can be seen that the PCTF for the Type 1 system is given by

$$\begin{aligned} C(n_x, n_y; n_x', n_y') = \iint \int_{-\infty}^{\infty} \iint & \; h_1(x_o, y_o)\; h_1^*(x_o', y_o')\; g_2(x_o - x_o', y_o - y_o') \\ & \cdot \exp\{-2p\, j(n_x x_o + n_y y_o)\} \exp\{2p\, j(n_x' x_o' + n_y' y_o')\} \\ & \cdot dx_o\, dy_o\, dx_o'\, dy_o' \end{aligned} \tag{3.34}$$

which by substituting for $g_2(x_o, y_o)$ from eq. (3.11) and rearranging gives

$$\begin{aligned} C(n_x, n_y; n_x', n_y') = \iint \int_{-\infty}^{\infty} \iint & \; h_1(x_o, y_o) h_1^*(x_o', y_o') \left| p_2(x_2, y_2) \right|^2 \\ & \cdot \exp\{-2p\, j(n_x x_o + n_y y_o)\} \exp\{2p\, j(n_x' x_o' + n_y' y_o')\} \\ & \cdot \exp\left\{\frac{2p\, j}{l\, f}(x_2 x_o - x_2 x_o' + y_2 y_o - y_2 y_o')\right\} \\ & \cdot dx_o\, dy_o\, dx_o'\, dy_o'\, dx_2\, dy_2 \end{aligned} \quad . \tag{3.35}$$

Combining the terms in the exponentials and separating the variables, allows eq. (3.35) to be recast in the form

$$\begin{aligned} C(n_x, n_y; n_x', n_y') = & \int_{-\infty}^{\infty} \iint \left| p_2(x_2, y_2) \right|^2 \\ & \cdot \left\{ \int_{-\infty}^{\infty} \iint h_1(x_o, y_o) \exp\left\{-2p\, j\left(x_o\left[n_x - \frac{x_2}{l\, f}\right] + y_o\left[n_y - \frac{y_2}{l\, f}\right]\right)\right\} dx_o dy_o \right\} \quad . \\ & \cdot \left\{ \int_{-\infty}^{\infty} \iint h_1^*(x_o', y_o') \exp\left\{2p\, j\left(x_o'\left[n_x' - \frac{x_2}{l\, f}\right] + y_o'\left[n_y' - \frac{y_2}{l\, f}\right]\right)\right\} dx_o' dy_o' \right\} dx_2\, dy_2 \end{aligned} \tag{3.36}$$

Using the shift and convolution theorems [42,43] now allows the Type 1 PCTF to be expressed in terms of the objective and collector aperture pupil functions, i.e.

$$C\left(n_x, n_y; n_x', n_y'\right) = \iint_{-\infty}^{\infty} p_1\left(n_x\, l\, f - x_2, n_y\, l\, f - y_2\right) p_1{}^*\left(n_x'\, l\, f - x_2, n_y'\, l\, f - y_2\right) \cdot \left|p_2\left(x_2, y_2\right)\right|^2 \, dx\, dy \tag{3.37}$$

where scaling terms have been ignored.

If it assumed that the objective and collector apertures are symmetrical about the *x* and *y* axes, then the time reversal of p_1 and $p_1{}^*$ in eq. (3.37) can be ignored, such that the Type 1 PCTF may be written in the more usual form

$$C\left(n_x, n_y; n_x', n_y'\right) = \iint_{-\infty}^{\infty} p_1\left(x + n_x\, l\, f, y + n_y\, l\, f\right) p_1{}^*\left(x + n_x'\, l\, f, y + n_y'\, l\, f\right) \cdot \left|p_2\left(x, y\right)\right|^2 \, dx\, dy \tag{3.38}$$

where the symbols have their usual meaning.

It can be seen from eq. (3.38) that the generation of the Type 1 PCTF is effectively a correlation type process involving the objective aperture pupil function, its complex conjugate and the square magnitude of the collector aperture pupil function [4,7,20,34]. A computational procedure for generating the Type 1 PCTF will be described in detail in sec. 6.1.

The response of the Type 1 reflectance scanning microscope can now be calculated in two ways, either directly via eq. (3.10) or using the transfer function representation of eq. (3.32). These methods have been implemented in computer code and are termed the ‘direct calculation’ approach and the ‘transfer function’ approach. In the ‘direct calculation’ approach the electric field is calculated as it propagates through the optical system as the sample is scanned beneath the focused spot. It may be used for generating the response to simple one-dimensional and two-dimensional reflectance type objects, and is described in detail in sec. 5.1. In the ‘transfer function’ approach the response is generated using the transfer function representation of the signal and is described in sec. 6.2 for generating the response to simple one-dimensional reflectance type objects.

3.3 The Type 2, or confocal, reflectance scanning microscope

It has been described in chapter 1 that an alternative scanning microscope arrangement can be configured by placing a pinhole arrangement into the detection arm of the instrument. The Type 2, or confocal scanning microscope, as it is commonly referred, has found widespread use in biological spheres, where its depth discrimination properties are primarily useful [4,53]. The introduction of a confocal pinhole into the detection arm of the instrument leads to a modification of the imaging characteristics of the scanning microscope. To understand the imaging process in the confocal microscope, and to compare its imaging characteristics with those of the Type 1 configuration, it is useful to develop a similar mathematical description of imaging in such an optical configuration. The analysis follows directly from that presented for the Type 1 configuration, as described in sec. 3.1, and involves the calculation of the electric field as it propagates through the optical system.

Optical configurations

The confocal reflectance scanning microscope can be implemented using the two configurations which are illustrated in Figs. 3.8 and 3.9.

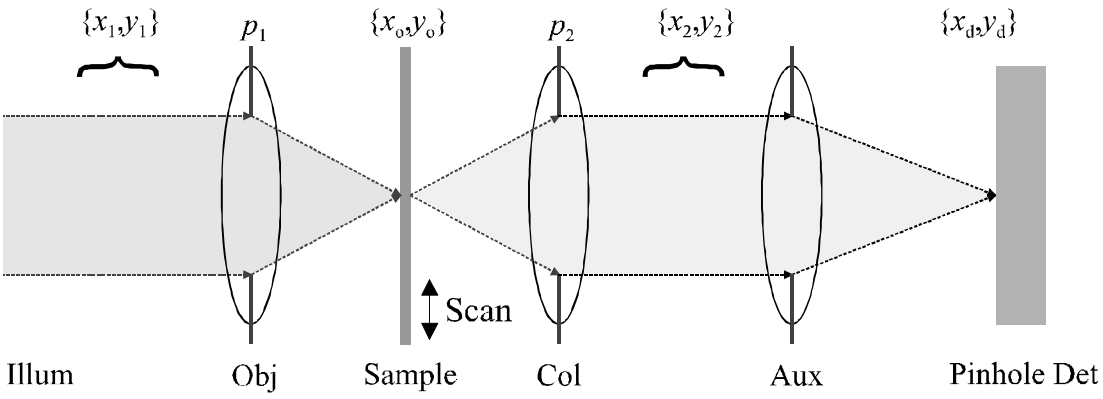

Figure 3.8 : *The optical layout of the ordinary Type 2, or confocal, reflectance scanning microscope, employing a pinhole photo-detector.*

Figure 3.8 illustrates the confocal reflectance scanning microscope where the pinhole aperture is introduced by replacing the large area photo-detector of the Type 1 system with an auxiliary lens and pinhole photo-detector arrangement. The auxiliary lens is used to focus the propagating field that is reflected from the sample, onto the plane of the pinhole photo-detector. The pinhole photo-detector can be visualised as either a photo-detector of infinitesimally small extent, or a large area photo-detector with a pinhole aperture placed immediately in front of it.

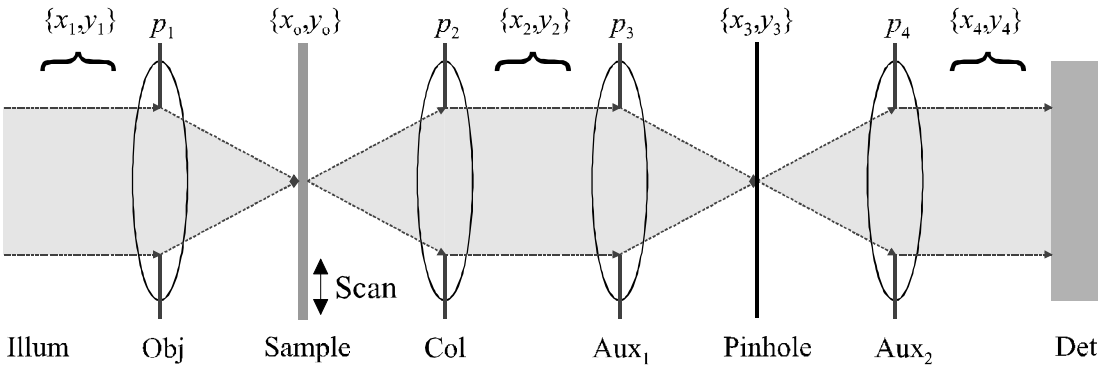

Figure 3.9 : *The optical layout of the ordinary Type 2, or confocal, reflectance scanning microscope, employing a pinhole aperture and auxiliary lens arrangement.*

Figure 3.9 illustrates an alternative confocal detection arrangement where a pinhole aperture is placed in the combined focal point of two auxiliary lenses. The propagating field that is reflected from the sample is brought to focus in the plane of the pinhole aperture by the first auxiliary lens, the field then propagates through the pinhole and diverges towards to second auxiliary lens. Here the field is collimated and continues to propagate, without further modification, to the large area photo-detector, which is assumed to be of uniform responsivity.

Due to the complexities involved in fabricating a pinhole photo-detector, the confocal arrangement illustrated in Fig. 3.9 is the more realistic system to implement practically.

It is instructive to analyse both the confocal imaging systems illustrated in Fig. 3.8 and Fig. 3.9 to determine if both systems exhibit identical imaging characteristics.

Image calculation

In order to analyse the signal generation process in the confocal reflectance scanning microscope, the field distribution incident on the photo-detector has to be calculated for a known incident field distribution on the objective aperture, as in the Type 1 configuration.

Consider first the confocal configuration of Fig. 3.8. The field, $y'(x_2, y_2)$, in the plane of the auxiliary lens is as calculated previously in the Type 1 system, as given by eq. (3.4). Immediately after the auxiliary lens the field distribution, $y''(x_2, y_2)$, is modified by the aperture pupil function of the auxiliary lens, $p_3(x_2, y_2)$, to give

$$y''(x_2, y_2) = y(x_2, y_2) p_2(x_2, y_2) p_3(x_2, y_2) \quad . \tag{3.39}$$

The field distribution, $y(x_d, y_d)$, incident on the photo-detector is given by the two-dimensional Fourier transform of the field distribution $y''(x_2, y_2)$, immediately after the auxiliary lens, i.e.

$$\begin{aligned} y(x_d, y_d) = \frac{1}{l f_A} \iint_{-\infty}^{\infty} & \left(y(x_2, y_2) p_2(x_2, y_2) p_3(x_2, y_2) \right) \\ & \cdot \exp\left\{ \frac{jk}{f_A} (x_d x_2 + y_d y_2) \right\} dx_2 dy_2 \end{aligned} \tag{3.40}$$

where f_A is the focal length of the auxiliary lens, $\{x_d, y_d\}$is the plane of the photo-detector and all other symbols have their usual meaning. The signal from the photo-detector is again given by the integral, over the area of the photo-detector, of the square magnitude of the incident distribution, i.e.

$$I(x_s, y_s) = \iint_{-\infty}^{\infty} \left| y(x_d, y_d) \right|^2 R(x_d, y_d) dx_d dy_d \tag{3.41}$$

or

$$I(x_s, y_s) = \iint_{-\infty}^{\infty} y(x_d, y_d) y^*(x_d, y_d) R(x_d, y_d) dx_d dy_d \tag{3.42}$$

where $R(x_d, y_d)$ represents the responsivity of the photo-detector and * represents complex conjugation. Substituting for $y(x_d, y_d)$ from eq. (3.40) allows eq. (3.42) to be recast in the form

$$
\begin{aligned}
I(x_s, y_s) = \iint \iint_{-\infty}^{\infty} & \; y(x_2, y_2) y^*(x_2', y_2') \\
& \cdot p_2(x_2, y_2) p_2^*(x_2', y_2') p_3(x_2, y_2) p_3^*(x_2', y_2') \\
& \cdot \iint_{-\infty}^{\infty} R(x_d, y_d) \exp\left\{ \frac{jk}{f_A} \left(x_d (x_2 - x_2') x_2 + y_d (y_2 - y_2') \right) \right\} dx_d dy_d \\
& \cdot dx_2 dy_2 dx_2' dy_2'
\end{aligned}
\tag{3.43}
$$

which simplifies to give

$$
\begin{aligned}
I(x_s, y_s) = \iint \iint_{-\infty}^{\infty} & \; y(x_2, y_2) y^*(x_2', y_2') p_c(x_2, y_2) p_c^*(x_2', y_2') \\
& \cdot G(x_2 - x_2', y_2 - y_2') \, dx_2 dy_2 dx_2' dy_2'
\end{aligned}
\tag{3.44}
$$

where $G(x_2, y_2)$ is the Fourier transform of the pinhole photo-detector responsivity, i.e.

$$
G(x_2, y_2) = \iint_{-\infty}^{\infty} R(x_d, y_d) \exp\left\{ \frac{jk}{f_A} (x_d x_2 + y_d y_2) \right\} dx_d dy_d \tag{3.45}
$$

and $p_c(x_2, y_2)$ is the combined aperture pupil function of the collector and auxiliary lenses, i.e.

$$
p_c(x_2, y_2) = p_2(x_2, y_2) p_3(x_2, y_2) \; . \tag{3.46}
$$

Substituting for $y(x_2, y_2)$ from eq. (3.3) allows eq. (3.44) to be expressed in terms of the reflectance properties of the sample, i.e.

$$
\begin{aligned}
I(x_s, y_s) = \iint \iint_{-\infty}^{\infty} & \; h_1(x_o, y_o) h_1^*(x_o', y_o') r(x_o - x_s, y_o - y_s) r^*(x_o' - x_s, y_o' - y_s) \\
& \cdot \iint \iint_{-\infty}^{\infty} p_c(x_2, y_2) p_c^*(x_2', y_2') G(x_2 - x_2', y_2 - y_2') \\
& \cdot \exp\left\{ \frac{jk}{f} (x_2 x_o + y_2 y_o) \right\} \exp\left\{ \frac{-jk}{f} (x_2' x_o' + y_2' y_o') \right\} dx_2 dy_2 dx_2' dy_2' \\
& \cdot dx_o dy_o dx_o' dy_o'
\end{aligned}
\tag{3.47}
$$

This can be rewritten as

$$
\begin{aligned}
I(x_s, y_s) = \iint \iint_{-\infty}^{\infty} & \; h_1(x_o, y_o) h_1^*(x_o', y_o') r(x_o - x_s, y_o - y_s) r^*(x_o' - x_s, y_o' - y_s) \\
& \cdot g(x_o, y_o; x_o', y_o') dx_o dy_o dx_o' dy_o'
\end{aligned}
\tag{3.48}
$$

where $g(x_o, y_o; x_o', y_o')$ is given by

$$g(x_o, y_o; x_o', y_o') = \iint_{-\infty}^{\infty} p_c(x_2, y_2) p_c^*(x_2', y_2') G(x_2 - x_2', y_2 - y_2') \cdot \exp\left\{\frac{jk}{f}(x_2 x_o + y_2 y_o)\right\} \exp\left\{\frac{-jk}{f}(x_2' x_o' + y_2' y_o')\right\} dx_2 dy_2 dx_2' dy_2' \tag{3.49}$$

where all symbols have their usual meaning and constant scaling factors have been ignored.

It can be seen that the signal generation process for the confocal reflectance system is again a convolution type operation. However, it is more complicated than the Type 1 imaging process in so much as it now incorporates properties of the auxiliary lens and pinhole photo-detector.

Presenting now the analysis for the alternative confocal reflectance system illustrated in Fig 3.9. The field, $y''(x_2, y_2)$, immediately after auxiliary lens 1 is given by

$$y''(x_2, y_2) = y(x_2, y_2) p_2(x_2, y_2) p_3(x_2, y_2) \tag{3.50}$$

where $p_3(x_2, y_2)$ represents the aperture pupil function of auxiliary lens 1, and $p_2(x_2, y_2)$ is the collector aperture pupil function. The field distribution, $y(x_3, y_3)$, in the plane of the pinhole is given by the two-dimensional Fourier transform of the field distribution, $y''(x_2, y_2)$, immediately after auxiliary lens 1, i.e.

$$y(x_3, y_3) = \frac{1}{l f_{A1}} \iint_{-\infty}^{\infty} \left(y(x_2, y_2) p_2(x_2, y_2) p_3(x_2, y_2)\right) \cdot \exp\left\{\frac{jk}{f_{A1}}(x_3 x_2 + y_3 y_2)\right\} dx_2 dy_2 \tag{3.51}$$

where f_{A1} is the focal length of auxiliary lens 1, and all the other symbols have their usual meaning. Immediately after the pinhole aperture the field is modified by the pupil function of the pinhole, $p_p(x_3, y_3)$, to give

$$y'(x_3, y_3) = p_p(x_3, y_3) y(x_3, y_3) \ . \tag{3.52}$$

The field, $y(x_4, y_4)$, in the plane of auxiliary lens 2 is given by the two-dimensional Fourier transform of the field, $y'(x_3, y_3)$, immediately after the pinhole, i.e.

$$y(x_4, y_4) = \frac{1}{l f_{A2}} \iint_{-\infty}^{\infty} y'(x_3, y_3) \exp\left\{\frac{jk}{f_{A2}}(x_4 x_3 + y_4 y_3)\right\} dx_3 dy_3 \tag{3.53}$$

where f_{A2} is the focal length of auxiliary lens 2, and all the other symbols have their usual meaning. Immediately after auxiliary lens 2 the field is modified by the aperture pupil function of auxiliary lens 2, $p_4(x_4, y_4)$, to give

$$y'(x_4, y_4) = p_4(x_4, y_4) y(x_4, y_4) \quad . \tag{3.54}$$

The field then propagates, without further modification, towards the photo-detector. The signal from the photo-detector is calculated as previously, and is given by

$$I(x_s, y_s) = \iint_{-\infty}^{\infty} \left| y'(x_4, y_4) \right|^2 dx_d dy_d \tag{3.55}$$

where it is assumed the responsivity is uniform (equal to unity) over the area of the photo-detector. Substituting for $y'(x_4, y_4)$ from eq. (3.54) into eq. (3.55) gives

$$I(x_s, y_s) = \iint_{-\infty}^{\infty} y(x_4, y_4) y^*(x_4, y_4) \left| p_4(x_4, y_4) \right|^2 dx_4 dy_4 \tag{3.56}$$

which by substituting for $y(x_4, y_4)$ using eq. (3.53) and rearranging gives

$$\begin{aligned} I(x_s, y_s) = \iint_{-\infty}^{\infty} \iint_{-\infty}^{\infty} & y'(x_3, y_3) y'^*(x_3', y_3') \\ & \cdot \iint_{-\infty}^{\infty} \left| p_4(x_4, y_4) \right|^2 \exp\left\{ \frac{jk}{f_{A2}} \left(x_4 (x_3 - x_3') + y_4 (y_3 - y_3') \right) \right\} dx_4 dy_4 \quad . \\ & \cdot dx_3 dy_3 dx_3' dy_3' \end{aligned} \tag{3.57}$$

If it assumed that auxiliary lens 2 collects all the field that propagates through the confocal pinhole, and that it does not obstruct the field in any way, then $p_4(x_4, y_4)$ can be assumed to be uniform (equal to unity) for all $\{x_4, y_4\}$ and eq. (3.57) simplifies to give

$$I(x_s, y_s) = \iint_{-\infty}^{\infty} y'(x_3, y_3) y'^*(x_3, y_3) dx_3 dy_3 \tag{3.58}$$

which substituting for $y'(x_3, y_3)$ from eq. (3.52) gives

$$I(x_s, y_s) = \iint_{-\infty}^{\infty} y(x_3, y_3) y^*(x_3, y_3) \left| p_p(x_3, y_3) \right|^2 dx_3 dy_3 \ . \tag{3.59}$$

Substituting for $y(x_3, y_3)$ from eq. (3.51) and rearranging gives

$$
\begin{aligned}
I(x_s, y_s) = \iint\limits_{-\infty}^{\infty} & \; y(x_2, y_2) y^*(x_2', y_2') \\
& \cdot p_2(x_2, y_2) p_2^*(x_2', y_2') p_3(x_2, y_2) p_3^*(x_2', y_2') \\
& \cdot \iint\limits_{-\infty}^{\infty} \left| p_p(x_3, y_3) \right|^2 \exp\left\{ \frac{jk}{f_{A1}} \left(x_3(x_2 - x_2') + y_3(y_2 - y_2') \right) \right\} dx_3 dy_3 \\
& \cdot dx_2 dy_2 dx_2' dy_2'
\end{aligned}
\tag{3.60}
$$

which can be further simplified to give

$$
\begin{aligned}
I(x_s, y_s) = \iint\limits_{-\infty}^{\infty} & \; y(x_2, y_2) y^*(x_2', y_2') p_c(x_2, y_2) p_c^*(x_2', y_2') \\
& \cdot G(x_2 - x_2', y_2 - y_2') \, dx_2 dy_2 dx_2' dy_2'
\end{aligned}
\tag{3.61}
$$

where $G(x_2, y_2)$ is the Fourier transform of the square magnitude of the pinhole aperture pupil function, i.e.

$$
G(x_2, y_2) = \iint\limits_{-\infty}^{\infty} \left| p_p(x_3, y_3) \right|^2 \exp\left\{ \frac{jk}{f_{A1}} (x_3 x_2 + y_3 y_2) \right\} dx_3 dy_3 \tag{3.62}
$$

and $p_c(x_2, y_2)$ is the combined aperture pupil function of the collector and auxiliary lenses as given by eq. (3.46). Substituting for $y(x_2, y_2)$ from eq. (3.3) allows eq. (3.61) to be expressed in terms of the reflectance properties of the sample, i.e.

$$
\begin{aligned}
I(x_s, y_s) = \iint\limits_{-\infty}^{\infty} & \; h_1(x_o, y_o) h_1^*(x_o', y_o') r(x_o - x_s, y_o - y_s) r^*(x_o' - x_s, y_o' - y_s) \\
& \cdot \iint\limits_{-\infty}^{\infty} p_c(x_2, y_2) p_c^*(x_2', y_2') G(x_2 - x_2', y_2 - y_2') \\
& \cdot \exp\left\{ \frac{jk}{f} (x_2 x_o + y_2 y_o) \right\} \exp\left\{ \frac{-jk}{f} (x_2' x_o' + y_2' y_o') \right\} dx_2 dy_2 dx_2' dy_2' \\
& \cdot dx_o dy_o dx_o' dy_o'
\end{aligned}
\tag{3.63}
$$

which can be rewritten as

$$
\begin{aligned}
I(x_s, y_s) = \iint\limits_{-\infty}^{\infty} & \; h_1(x_o, y_o) h_1^*(x_o', y_o') r(x_o - x_s, y_o - y_s) r^*(x_o' - x_s, y_o' - y_s) \\
& \cdot g(x_o, y_o; x_o', y_o') dx_o dy_o dx_o' dy_o'
\end{aligned}
\tag{3.64}
$$

where $g(x_o, y_o; x_o', y_o')$ is given by eq. (3.49) with $G(x_2, y_2)$ given by eq. (3.62), all other symbols have their usual meaning and constant scaling factors have been ignored.

Comparing eq. (3.48) and eq. (3.64) it can be seen that the two confocal configurations illustrated in Figs 3.8 and 3.9 have exactly the same imaging characteristics, providing auxiliary lens 2 in Fig. 3.9 collects all the field that propagates through the pinhole.

It is instructive at this point to consider two extreme cases of pinhole size for the configuration of Fig. 3.9. If the pinhole aperture is infinitely large, such that $p_p(x_3, y_3) = 1$ for all $\{x_3, y_3\}$, then

$$G(x_2, y_2) = d(x_2, y_2) \tag{3.65}$$

and eq. (3.64) reduces to the same form as that for the Type 1 reflectance system, eq. (3.10), as would be expected.

If the pinhole is infinitesimally small, such that $p_p(x_3, y_3) = d(x_3, y_3)$, then

$$G(x_2, y_2) = 1 \tag{3.66}$$

and

$$g(x_o, y_o; x_o', y_o') = h_c(x_o, y_o) h_c{}^*(x_o', y_o') \tag{3.67}$$

which allows the signal to be expressed in the form

$$I(x_s, y_s) = \left| \iint_{-\infty}^{\infty} h_1(x_o, y_o) h_c(x_o, y_o) r(x_o - x_s, y_o - y_s) dx_o dy_o \right|^2 \tag{3.68}$$

and the confocal imaging system exhibits coherent imaging properties, and is termed the ***ideal*** confocal system. Note, the form of the collector lens point spread function now effects the imaging process, unlike the Type 1 configuration.

Transfer function representation

As in the Type 1 reflectance scanning microscope analysis, it is possible to develop a transfer function representation of the signal from the confocal reflectance scanning microscope.

Recalling eq. (3.29) and eq. (3.30), the reflectance properties of the sample can be expressed in terms of its spatial frequency spectrum, $\Gamma(n_x, n_y)$, i.e.

$$r(x,y)=\iint_{-\infty}^{\infty}\Gamma(n_x,n_y)\exp\left(-2p\,j\left[n_x x+n_y y\right]\right)dn_x dn_y \tag{3.29}$$

and its complex conjugate

$$r^*(x',y')=\iint_{-\infty}^{\infty}\Gamma^*(n_x',n_y')\exp\left(2p\,j\left[n_x' x'+n_y' y'\right]\right)dn_x' dn_y' \tag{3.30}$$

which substituting into eq. (3.64) gives

$$\begin{aligned}I(x_s,y_s)=\iint_{-\infty}^{\infty}\Bigg[&\iint_{-\infty}^{\infty}h_1(x_o,y_o)\,h_1^*(x_o',y_o')\,g_2(x_o,y_o;x_o',y_o')\\&\cdot\exp\left\{-2p\,j\left(n_x x_o-n_x' x_o'+n_y y_o-n_y' y_o'\right)\right\}dx_o\,dy_o\,dx_o'\,dy_o'\Bigg]\\&\cdot\Gamma(n_x,n_y)\Gamma^*(n_x',n_y')\exp\left\{-2p\,j\left(\left(n_x-n_x'\right)x_s+\left(n_y-n_y'\right)y_s\right)\right\}\\&\cdot dn_x\,dn_y\,dn_x'\,dn_y'\end{aligned} \tag{3.69}$$

where the symbols have their usual meaning. Replacing the term in square brackets of eq. (3.69) with $C(n_x,n_y;n_x',n_y')$, the signal from the confocal reflectance system can be expressed in the characteristic form given previously in eq. (3.32), i.e.

$$\begin{aligned}I(x_s,y_s)=\iint_{-\infty}^{\infty}&C(n_x,n_y;n_x',n_y')\,M(n_x,n_y;n_x',n_y')\\&\cdot\exp\left\{2p\,j\left[\left(n_x-n_x'\right)x_s+\left(n_y-n_y'\right)y_s\right]\right\}dn_x\,dn_y\,dn_x'\,dn_y'\end{aligned} \tag{3.32}$$

where for the case of the confocal system the term $C(n_x,n_y;n_x',n_y')$ represents the confocal PCTF, and the medium function $M(n_x,n_y;n_x',n_y')$ remains unchanged.

The confocal PCTF

Comparing eq. (3.32) and eq. (3.69) it can be seen that the confocal PCTF is given by

$$\begin{aligned}C(n_x,n_y;n_x',n_y')=\iint_{-\infty}^{\infty}&h_1(x_o,y_o)\,h_1^*(x_o',y_o')\,g_2(x_o,y_o;x_o',y_o')\\&\cdot\exp\left\{-2p\,j\left(n_x x_o+n_y y_o\right)\right\}\exp\left\{2p\,j\left(n_x' x_o'_o+n_y' y_o'\right)\right\}dx_o\,dy_o\,dx_o'\,dy_o'\end{aligned} \tag{3.70}$$

that by substituting for $g_2(x_2, y_2; x_2', y_2')$ using eq. (3.49) and rearranging gives

$$C(n_x, n_y; n_x', n_y') = \iint\iint\iint_{-\infty}^{\infty}\iint\iint h_1(x_o, y_o)\, h_1^*(x_o', y_o') \cdot p_c(x_2, y_2) p_c^*(x_2', y_2') G(x_2 - x_2', y_2 - y_2') \cdot \exp\left\{\frac{jk}{f}(x_2 x_o + y_2 y_o)\right\} \exp\left\{\frac{-jk}{f}(x_2' x_o' + y_2' y_o')\right\} dx_2 dy_2 dx_2' dy_2' \cdot \exp\left\{-2pj\,(n_x x_o + n_y y_o)\right\} \exp\left\{2pj\,(n_x' x_o'_o + n_y' y_o')\right\} dx_o\, dy_o\, dx_o'\, dy_o' \tag{3.71}$$

Grouping the terms in the exponentials and rearranging gives

$$C(n_x, n_y; n_x', n_y') = \iint_{-\infty}^{\infty}\iint p_c(x_2, y_2) p_c^*(x_2', y_2') G(x_2 - x_2', y_2 - y_2') \cdot \iint_{-\infty}^{\infty} h_1(x_o, y_o) \exp\left\{-2pj\left(x_o\left[n_x - \frac{x_2}{lf}\right] + y_o\left[n_y - \frac{y_2}{lf}\right]\right)\right\} dx_o\, dy_o \cdot \iint_{-\infty}^{\infty} h_1^*(x_o', y_o') \exp\left\{2pj\left(x_o'\left[n'_x - \frac{x_2'}{lf}\right] + y_o'\left[n_y' - \frac{y_2'}{lf}\right]\right)\right\} dx_o'\, dy_o' \cdot dx_2 dy_2 dx_2' dy_2' \tag{3.72}$$

which by using the shift and convolution theorems [42,43] allows the confocal PCTF to be expressed in the form

$$C(n_x, n_y; n_x', n_y') = \iint_{-\infty}^{\infty}\iint p_1(x + n_x lf, y + n_y lf) p_1^*(x' + n_x' lf, y' + n_y' lf) \cdot p_c(x, y) p_c^*(x', y') G(x - x', y - y') dx dy dx' dy' \tag{3.73}$$

where $G(x, y)$ is given by eq. (3.62) and all other symbols have their usual meaning and it is assumed the apertures are symmetrical about the *x* and *y* axes.

It can be seen that the expressions representing the signal from both the Type 1 and confocal reflectance scanning microscopes are of identical form. However, the PCTFs of the two imaging configurations are very different. Comparing eq. (3.38) and eq. (3.73) it can be seen that the confocal PCTF is more complicated compared to the Type 1 PCTF, in so much that the confocal PCTF is a function of the Fourier

transform of the square modulus of the pinhole aperture pupil function, and is a convolution process involving four variables.

Again consider two extreme cases of confocal pinhole aperture size. For the case where the confocal pinhole is infinitesimally small, such that $p_p(x_3, y_3) = d(x_3, y_3)$, then $G(x - x', y - y')$=1 and eq. (3.73) reduces to the form,

$$C\left(n_x, n_y; n_x', n_y'\right) = \left| \iint_{-\infty}^{\infty} p_1\left(x + n_x lf, y + n_{yx} lf\right) p_c(x, y) dxdy \right|^2 \tag{3.74}$$

and the confocal PCTF is effectively given by the square magnitude of the incoherent OTF [4].

For the case where the confocal pinhole is infinitely large, such that $p_p(x_3, y_3) = 1$ for all $\{x_3, y_3\}$, then in such a case $G(x - x', y - y')$ is a delta function and eq. (3.73) reduces to the form,

$$\begin{aligned} C\left(n_x, n_y; n_x', n_y'\right) = \iint_{-\infty}^{\infty} \iint & p_1\left(x + n_x lf, y + n_{yx} lf\right) p_1{}^*\left(x + n_x' lf, y + n_y' lf\right) \\ & \cdot p_c(x, y) p_c{}^*(x, y) dxdy \end{aligned} \tag{3.75}$$

which is the same form as for the Type 1 case, as would be expected.

Chapters 5 and 6 described computational procedures for evaluating the imaging equations developed throughout this current chapter.